Ultrafast carrier and phonon dynamics in Bi_2Se_3 under high pressure

Y. Yang,[1,2,*] Y. H. Meng,[2,*] B. R. Lu,[2] F. Jin,[2] Y. G. Shi,[2] F. Hong,[2] S. S. Zhang,[1,3,†] X. H. Yu,[2,‡] X. B. Wang,[2,§] and J. L. Luo[2]

[1]*Key Laboratory of Education Ministry for Laser and Infrared System Integration Technology, Shandong University, Qingdao 266237, China*
[2]*Beijing National Laboratory for Condensed Matter Physics, Institute of Physics, Chinese Academy of Sciences, Beijing 100190, China*
[3]*School of Information Science and Engineering, Shandong University, Qingdao 266237, China*

(Received 1 November 2023; accepted 30 January 2024; published 16 February 2024)

The nonequilibrium carrier and phonon dynamics in Bi_2Se_3 was studied by a combination of Raman scattering and ultrafast optical pump-probe spectroscopy at high pressures up to 31 GPa. Detailed analysis reveals that the pressure dependence of the relaxation time and the damping rate of the A_{1g}^1 phonon mode exhibit an anomaly around 3 GPa supporting the occurrence of an electronic topological transition. At higher pressure, the transient reflectivity spectra manifest discontinuous changes around 11.5, 18.9, and 28 GPa, which can be assigned to the structure transitions as evidenced by the Raman spectra. Especially, low-frequency phonon modes, corresponding to the A_g phonon modes in the monoclinic $C2/m$ phase, were identified in both Raman and transient reflectivity spectra in the pressure range of 11.5 to 18.9 GPa. These results not only provide crucial insights into carrier-phonon interaction of Bi_2Se_3 under high pressure, but also pave the way for investigating the pressure-induced phase transitions from transient reflection spectroscopy.

DOI: 10.1103/PhysRevB.109.064307

I. INTRODUCTION

Topological insulators are a class of materials with gapless surface states and insulating bulk states. Due to the symmetry-protected band crossings with nontrivial topology on their surfaces, they are promising candidates as functional materials in future electronic and spintronic devices [1,2]. The dynamic properties of quasiparticles play a critical role in their potential applications. Bi_2Se_3 is a prototype three-dimensional topological insulator with the simplest possible surface band structure [3–5]. Therefore, this star compound provides an attractive platform to investigate the ultrafast quasiparticle dynamics in topological insulators [6–8].

Ultrafast optical pump-probe spectroscopy is a powerful tool for investigating the nonequilibrium quasiparticle dynamics by disentangling different decay processes in the time domain. It has been successfully employed to trace the relaxation processes of photoexcited quasiparticles in Bi_2Se_3 where multiple exponential decay components accompanied by oscillations have been observed [9–14]. The fast decay process occurring within a few picoseconds (ps) can be described by the two-temperature model, in which the relaxation time can be utilized to extract the electron-phonon (e-ph) coupling constant [15]. The thickness-dependent measurements have revealed interband relaxation involving surface states with a timescale of 5–220 ps, despite the simultaneous excitation of both bulk and surface states by the pump pulse [16,17]. In addition, high-frequency and low-frequency periodic oscillations in transient reflectivity are attributed to the coherent optical and acoustic phonons, respectively [18–20]. The temperature dependence of frequency and dephasing time of the optical phonon can be well described by the anharmonicity model [21,22], while the behavior of acoustic phonons can be explained by the strain pulse propagation model [23,24].

Recently, ultrafast spectroscopy has been extended to high-pressure conditions by combining with diamond anvil cell (DAC) techniques [25–27]. High pressure can provide an effective and clean way to precisely tune electronic and structural properties of materials. Bi_2Se_3 has a rhombohedral structure (space group $R\bar{3}m$) under ambient conditions. A pressure-induced electronic topological transition (ETT) or Lifshitz transition has been extensively observed at the pressure range from 3 to 5 GPa [28–30]. The ETT characterized by a topological change of the Fermi surface had been demonstrated by Raman scattering spectroscopy [30–32], x-ray diffraction [28,33], and transport experiments [34,35]. With further compression, Bi_2Se_3 was suggested to successively transform into monoclinic $C2/m$ and $C2/c$ structures at around 10 GPa and 20 GPa [29,31]. Subsequently, a fourth phase above 28 GPa was first assigned to the cubic $Im\bar{3}m$ phase and later to tetragonal $I4/mmm$ [29,32,36].

In this work, we combine ultrafast pump-probe spectroscopy and Raman spectroscopy to investigate the nonequilibrium quasiparticle dynamics in Bi_2Se_3 under pressures up to 31 GPa. Both the pressure dependence of the fast relaxation time and the damping rate of the A_{1g}^1 phonon mode give support to the observation of the ETT around 3 GPa. In addition, the carrier relaxation and coherent phonon modes exhibit discontinuous changes at 11.5, 18.9, and 28 GPa, respectively, which can be attributed to the structural phase transitions

*These authors contributed equally to this work.
†sasazhang@sdu.edu.cn
‡yuxh@iphy.ac.cn
§xinbowang@iphy.ac.cn

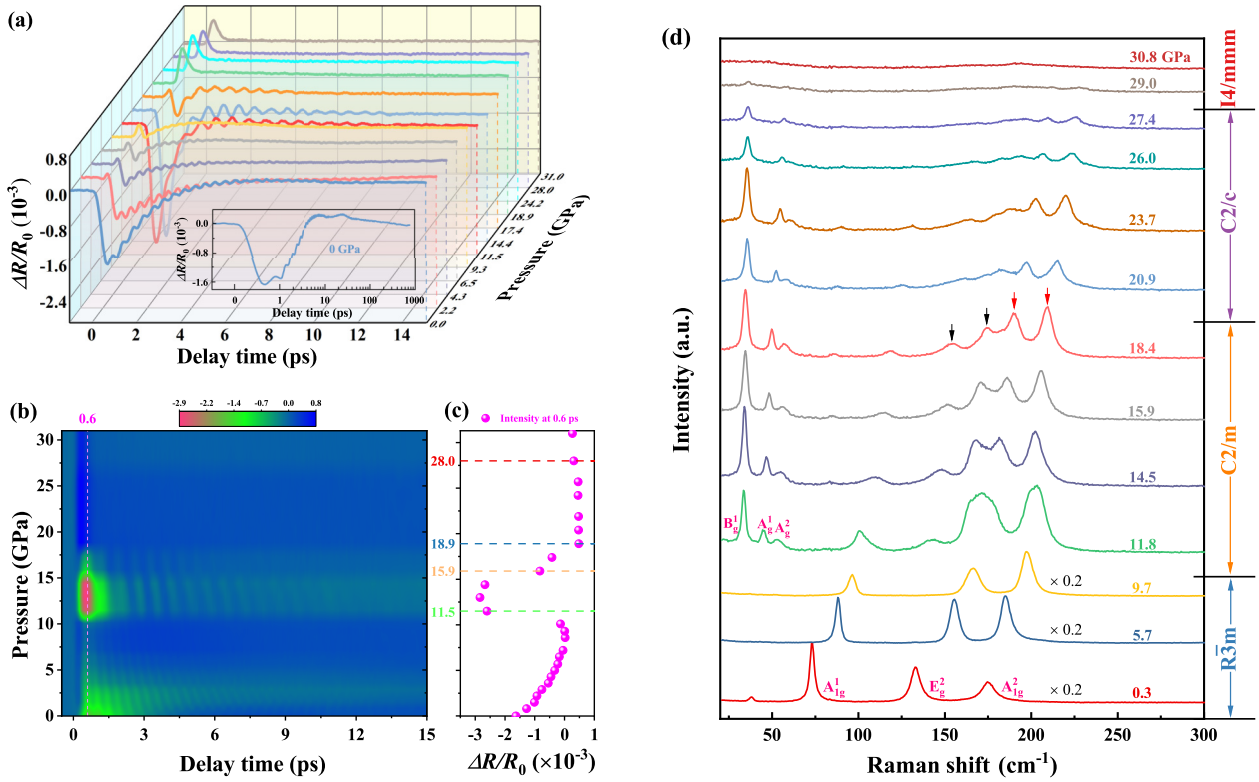

FIG. 1. (a) Transient reflectivity $\Delta R(t)/R_0$ in Bi_2Se_3 at different pressures. Inset: A logarithmic scale plot of the $\Delta R(t)/R_0$ signal under ambient conditions up to 780 ps. (b) Intensity map of the $\Delta R(t)/R_0$ for initial 15 ps. (c) Intensity of $\Delta R(t)/R_0$ at delay time of 0.6 ps as a function of pressure. (d) Raman spectra of Bi_2Se_3 at selected pressures. The spectra in the $R\bar{3}m$ phase are multiplied by 0.2 for the sake of clarity.

at these pressure points. Furthermore, two low-frequency phonon modes are identified in both the Raman spectra and optical pump-probe spectroscopy in the pressure range of 11.5 to 18.9 GPa. These results provide crucial insights into the pressure-induced changes in electronic topology and lattice structures from the ultrafast reflectivity spectra.

II. EXPERIMENTAL METHODS

Single crystals of Bi_2Se_3 were grown by the flux method. The optical pump probe spectroscopy under high pressure is similar to the setup described in Ref. [25]. The optical parametric amplifier (Orpheus F) seeded by a 50 kHz Yb:KGW amplifier (Pharos, Light Conversion) produced the laser pulses with wavelength of 800 nm and pulse duration of 60 femtoseconds. The laser pulses were split into pump and probe beams, with the former being converted into 400 nm pulses using a BBO crystal. The collinear pump and probe beams were focused onto the sample surface by using a 10× microscope lens with spot diameters of 25 and 14 μm, respectively. For all the measurements, the incident pump fluence was fixed at 120 $\mu J/cm^2$, and the probe fluence was approximately one order of magnitude smaller than that of pump. The relative reflectivity change of the probe beam was recorded by the balanced detection and lock-in amplifier. The quasihydrostatic pressure condition was achieved using a DAC with the culet size of 300 μm, in which KBr served as the pressure-transmitting medium. The newly exfoliated Bi_2Se_3 crystal was mounted in the DAC along with a ruby ball. The ruby fluorescence excited by a 532 nm CW laser was utilized for pressure calibration. The Raman spectra under high pressure were collected with a Jobin Yvon LabRam HR800 spectrometer equipped with a volume Bragg grating low-wave-number suite, a liquid-nitrogen-cooled back-illuminated charge-coupled device detector, and a 633 nm laser (Melles Griot). A background curve from KBr at ambient pressure was subtracted from the Raman spectra under compression.

III. RESULTS AND DISCUSSION

The relative change of reflectivity with respect to static reflectivity (R_0), i.e., $\Delta R(t)/R_0 = [R(t) - R_0]/R_0$, is recorded as a function of the delay time (t) between the pump and probe pulses. At ambient pressure, the $\Delta R(t)/R_0$ signal initially drops to a dip at 0.6 ps upon photoexcitation, followed by a rapid rise entangled with fast periodic oscillations. $\Delta R(t)/R_0$ exhibits a slow recovery on longer timescales and low-frequency oscillations in the time range of 8 to 50 ps. Such dynamics in Bi_2Se_3 outside the DAC have been widely studied, whereas the multiple exponential decay processes are attributed to the carrier relaxation process and the oscillations are assigned to the coherent phonon dynamics [12–18]. In the following, we mainly focus on the high-pressure evolution of the rich dynamics in Bi_2Se_3.

Figure 1(a) shows the $\Delta R(t)/R_0$ signals within an initial time window of 15 ps at representative pressures. The detailed experimental data are summarized as a 2D color map in Fig. 1(b). $\Delta R(t)/R_0$ changes significantly when the

pressure is applied to Bi_2Se_3. To visualize the pressure-induced variation of the photocarrier dynamics, the intensity at 0.6 ps is plotted in Fig. 1(c). As the pressure increases, the signal intensity gradually decreases to zero and suddenly changes to a negative value around 11.5 GPa. Thereafter, it changes little until 15.9 GPa and then decreases significantly. The dip at 0.6 ps evolves into a peak around 18.9 GPa, which remains almost constant, and then slightly decreases above 28 GPa. Meanwhile, the oscillations, manifested as stripes in the color map, become increasingly pronounced as pressure increases up to ~3 GPa, after which they remarkably weaken up to 10.1 GPa. Clearly, the oscillation period monotonically decreases in this pressure range. At 11.5 GPa, an appearance of a new oscillation with longer period is evidenced, which persists up to 15.9 GPa. With further compression, the oscillation gradually decreases and fully vanishes above 18.9 GPa.

Previous studies of Bi_2Se_3 have suggested the existence of pressure-induced ETT at 3–5 GPa, and a structural phase transition sequence of $R\bar{3}m \rightarrow C2/m \rightarrow C2/c \rightarrow Im\bar{3}m$ structures at 10, 20, and 28 GPa, respectively [28–30]. However, it was confirmed later that Bi_2Se_3 possesses $I4/mmm$ rather than $Im\bar{3}m$ phase at high pressure above 28 GPa [32,36]. The ETT can lead to a U-shaped pressure dependence of the linewidth (full width at half maximum) of optical phonon modes, which has been extensively observed in Raman experiments [30–32]. The occurrence of ETT near 3 GPa will be demonstrated through a detailed analysis of ultrafast spectroscopy. In order to confirm the pressure-induced structural phase transitions in Bi_2Se_3, the Raman spectroscopy at different pressures was measured. As shown in Fig. 1(d), three distinct peaks are observed at ambient $R\bar{3}$m structure, which can be assigned to the A_{1g}^1, E_g^2, and A_{1g}^2 modes, respectively [29,31,33,37]. The three modes manifest an obvious blueshift in frequency as pressure increases. Several new peaks emerge upon further compression to 11.8 GPa. Among them, the new modes around 33.5, 44.9, and 53.4 cm^{-1} are in good agreement with theoretical frequencies of B_g^1, A_g^1, and A_g^2 modes for $C2/m$ structure, respectively [29]. This implies a structural transition from the ambient $R\bar{3}m$ phase to the monoclinic $C2/m$ phase. Above 18.4 GPa, the Raman peaks located at 153.5 and 175.1 cm^{-1} [black arrows in Fig. 1(d)] broaden significantly and disappear at higher pressure. Besides, the intensity of the Raman peaks around 189.9 and 209.1 cm^{-1} [red arrows in Fig. 1(d)] decreases by half at 20.9 GPa. These results are in good agreement with the previous reports, corresponding to the structural transition from $C2/m$ to $C2/c$ phase [31,32,36]. The Raman modes are almost indistinguishable at pressures above 27.4 GPa, suggesting a structure transition into a body-centered tetragonal $I4/mmm$ phase [32,36].

Here we briefly discuss the potential impact of the pressure transmitting medium (KBr) on the phase transitions of Bi_2Se_3 under compression. It is known that KBr experiences a first-order phase transition that occurs at 2.3 GPa [38]. Actually, no discontinuity was observed around this pressure, neither in the transient reflectivity signals nor in the linewidths and the peak separation of ruby fluorescence spectra (not shown), indicating that the structure transition of KBr does not affect the ETT in Bi_2Se_3. In addition, it had been demonstrated that the appearance of the $C2/c$ phase of Bi_2Se_3 is very sensitive to the pressure environment, where it is absent under nonhydrostatic pressure conditions [32]. As we have discussed above, Bi_2Se_3 undergoes a clear $C2/m \rightarrow C2/c$ transition from the Raman spectra and the transient reflectivity data, suggesting that KBr provides a quasihydrostatic environment in our experiment. Based on these Raman results, the aforementioned discontinuous changes in ultrafast spectroscopy at 11.5, 18.9, and 28 GPa are probably related to pressure-induced structural phase transitions, which results in the change of electric band structure. In the following sections, we will discuss the decaying and oscillating components in succession.

A. Ultrafast decay processes

We first focus on the nonoscillatory part of the $\Delta R(t)/R_0$ signal that describes the photocarrier dynamics. Generally, the photoexcited carriers redistribute their energies through carrier-carrier scattering and thermalize to a quasi-Fermi-Dirac distribution with the temperature of electron T_e much higher than that of the lattice. Under ambient conditions, photoexcitation results in a sharp drop in $\Delta R(t)/R_0$ due to the carrier thermalization. The drop time of ~0.6 ps is longer than the expected value (~0.3 ps) for typical semiconductors and metals [39], which is consistent with the previous report in Bi_2Se_3 [13]. It was argued that the long drop time is attributed to the presence of a short-lived positive decay component, resulting from the ultrafast trapping of photocarriers by Se vacancies. It is worth noting that a small peak just after the photoexcitation emerges upon compression. Following the thermalization, these hot carriers transfer their excess energy to the lattice mainly through e-ph interaction, and finally establish a thermal equilibrium with the lattice. This process is referred to as the cooling or relaxation of hot carriers. In order to quantitatively analyze the carrier relaxation dynamics, we fit the $\Delta R(t)/R_0$ signals after first dip/peak using the following piecewise function:

$$\frac{\Delta R(t)}{R_0} = \begin{cases} A_{\text{fast}} e^{-\frac{t}{\tau_{\text{fast}}}} + A_{\text{slow}} e^{-\frac{t}{\tau_{\text{slow}}}} + C, & P \in (0, 10.1] \text{ or } [18.9, 31), \\ A_{\text{fast}} e^{-\frac{t}{\tau_{\text{fast}}}} + A_{\text{slow}} e^{-\frac{t}{\tau_{\text{slow}}}} + A_{\text{slowest}} e^{-\frac{t}{\tau_{\text{slowest}}}}, & P \in (10.1, 18.9), \end{cases} \quad (1)$$

where A and τ represent the amplitude and relaxation time of the nonoscillatory signal, respectively. The subscripts (fast, slow, and slowest) are used to denote different relaxation processes. C is a constant offset. As shown in Fig. 2, the fitted curves are in excellent agreement with the nonoscillating part of the experimental data over the entire pressure range. The pressure dependence of the extracted relaxation time of the slow decay τ_{slow} is very similar to τ_{fast}.

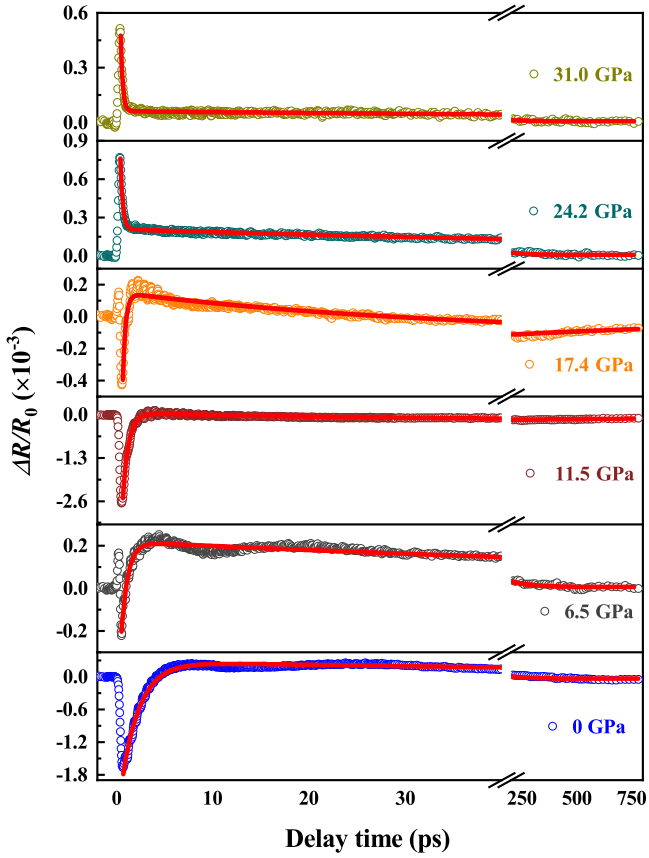

FIG. 2. $\Delta R(t)/R_0$ in Bi_2Se_3 at several selected pressures. The solid lines are fits to the nonoscillatory response using Eq. (1).

Therefore, we only discuss the fast relaxation in the following section.

The extracted relaxation time of the fast decay process (τ_{fast}) is presented in Fig. 3 as a function of pressure. Under ambient conditions, the relaxation time of ~1.9 ps is in accordance with the e-ph scattering time in angle-resolved photoemission spectroscopy [40] and optical pump-probe experiments in Bi_2Se_3 [19]. At low-pressure range, τ_{fast} quickly increases with increasing pressure until it reaches a maximum around 3 GPa, after which it starts to decrease quickly. In Bi_2Se_3, a pressure-induced ETT in the $R\bar{3}m$ phase was suggested at ~3 GPa, which results in a change in the topology of the Fermi surface that redistributes the electronic density of states (DOS) near the Fermi energy [28]. Therefore, the anomaly of τ_{fast} around this pressure is likely related to the sudden change of the electronic band structure across the ETT, which impacts the nonequilibrium carrier and phonon dynamics. The e-ph relaxation in Bi_2Se_3 can be described by the two-temperature model [15], that is, $\tau_{fast} = \pi k_B T_e/3\hbar\lambda\langle\omega^2\rangle$, where $\lambda\langle\omega^2\rangle$ is the second moment of the Eliashberg function that describes the strength of the e-ph interaction. The carrier density in Bi_2Se_3 increases on a logarithmic scale with applied pressure, which suggests the increase of electronic DOS near Fermi level [41], which would tend to promote a lower value of electron temperature T_e [42], thus resulting in a decreasing τ_{fast}. On the other hand, the electron-phonon interaction strength is closely connected with the dramatic change in the band structure. The strong sensitivity of the e-ph relaxation time τ_{fast} to pressure suggests the enhancement of electron phonon coupling across the ETT. Upon further compressing, the τ_{fast} decreases first and then increases slightly above 8 GPa. A similar pressure-induced feature is also observed in Sb_2Te_3, which was attributed to the semiconductor to semimetal transition [43,44]. As the pressure is increased from 10.1 to 18.9 GPa, τ_{fast} gradually decreases and then remains almost constant with further increases in pressure.

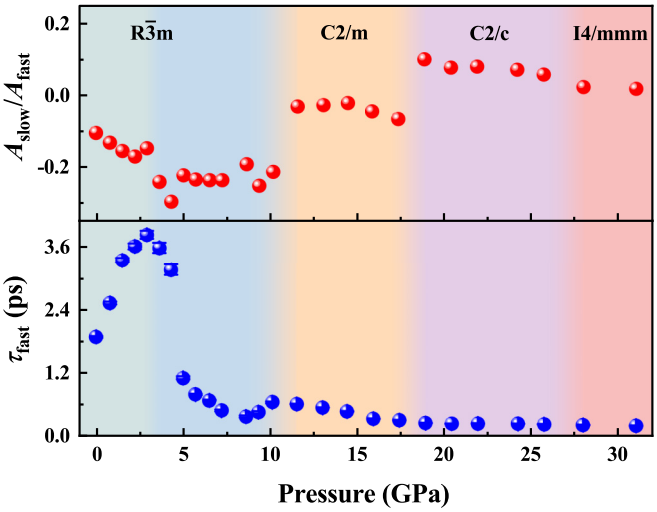

FIG. 3. Pressure dependence of the amplitude ratio A_{slow}/A_{fast} between the slow and fast processes and the fast relaxation time τ_{fast}.

To further clarify the pressure effect on the carrier dynamics, the amplitude ratio between the slow and fast processes, i.e., A_{slow}/A_{fast}, is plotted as a function of pressure in Fig. 3. The A_{slow}/A_{fast} decreases with increasing pressure up to ~3 GPa, after which it changes little in the $R\bar{3}m$ phase. Besides the anomaly caused by the ETT, A_{slow}/A_{fast} exhibits two discontinuous steps at 11.5 and 18.9 GPa, followed by a slight decrease above 28 GPa. It is noted that these abnormal pressure points coincide with the structure transitions of the aforementioned Raman results. The sudden increase of the weight of A_{fast} after the first phase transition may be caused by the sudden increase of carrier density around 11 GPa [35,45]. Especially, the amplitude of the fast relaxation component evolves from negative to positive above 18.9 GPa. These results suggest that the pressure-caused structure transition results in significant changes of the electric band structure, which finally impact the carrier relaxation processes.

B. Ultrafast coherent phonons

We now discuss the oscillatory components that describe the coherent phonon dynamics. The residual oscillations are extracted by subtracting the exponential decay background from the $\Delta R(t)/R_0$ signals, including high- and low-frequency oscillations which can be attributed to the coherent optical and acoustic phonon, respectively. A high-pass filter with a cutoff frequency of 1.2 THz was applied to remove the slowly varying component. Figure 4(a) shows several typical time-domain oscillations at selected pressures, while the pressure-dependent frequency-domain results are summarized in Fig. 4(b). It is obvious that the coherent

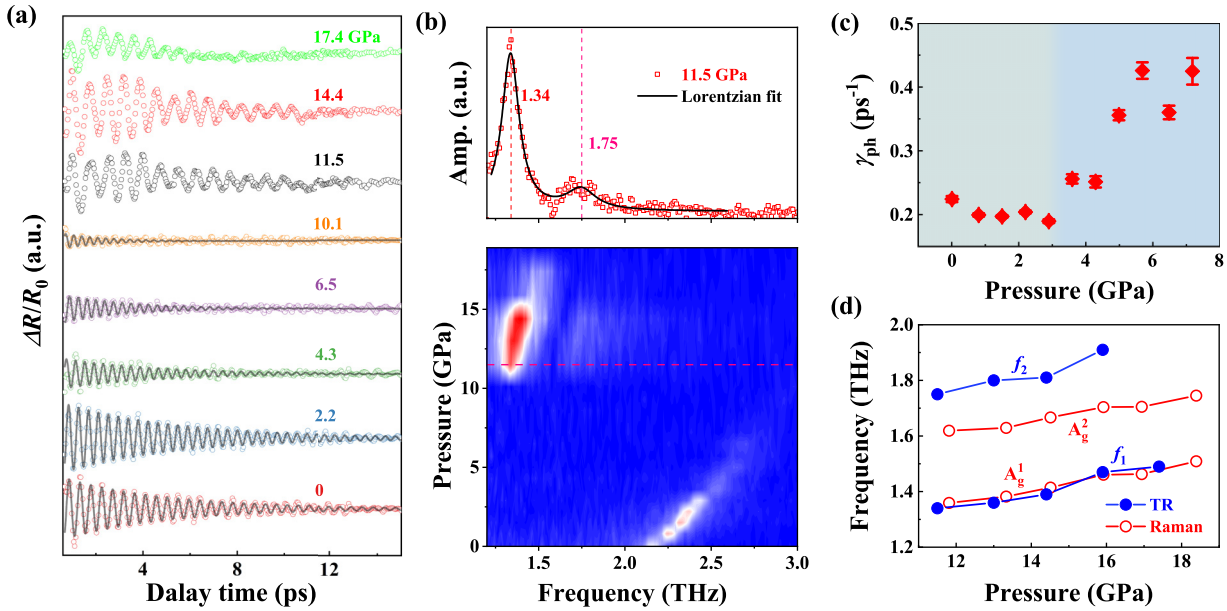

FIG. 4. (a) Extracted high-frequency oscillations at selected pressures. The black solid lines are the fits. (b) The Fourier-transformed spectra as a function of pressure in the frequency domain. The upper panel shows the spectrum at 11.5 GPa, where the solid line is a Lorentzian fit. (c) Damping rate ($\gamma_{\rm ph}$) of A^1_{1g} mode as a function of pressure in the $R\bar{3}m$ phase. (d) Optical phonon modes extracted from the transient reflectivity (TR) and Raman scattering spectra in the pressure range from 11.5 to 18.9 GPa.

phonon mode changes significantly above the pressure of the first structural transition.

In the $R\bar{3}m$ phase, the oscillations first strengthen with pressure up to 3 GPa and then disappear gradually up to around 10 GPa. To quantitatively analyze the properties of coherent optical phonons, the time-domain oscillatory signals were reproduced by a damped sinusoidal function in the form of $Be^{-t\gamma_{\rm ph}}\sin(2\pi f_o t+\varphi)$, where $\gamma_{\rm ph}$, B, f_o, and φ are the damping rate, amplitude, frequency, and initial phase, respectively. The fitting results are in good agreement with the experimental data, as shown in Fig. 4(a). The oscillation has a frequency of 2.16 THz at room pressure, which is consistent with the A^1_{1g} optical phonon frequency determined by the Raman scattering [29–33] and previous pump-probe spectroscopy [22–24]. The frequency increases monotonically with increasing pressure, as shown in Fig. 4(b). Since the A^1_{1g} mode corresponds to vibration along the c axis perpendicular to the layers [18,46], the interlayer distance decreases upon compression, enhancing interlayer coupling, and thereby resulting in a blueshift in frequency [37,47]. The fitted damping rate $\gamma_{\rm ph}$ initially decreases slightly with pressure up to 3 GPa and then increases under higher pressures, as depicted in Fig. 4(c). In previous Raman-scattering measurements, similar behaviors have been observed in the materials undergoing an ETT, where the linewidth of the Raman modes changes their slope crossing the ETT [30,48,49]. In principle, the damping rate (inverse of lifetime) of the optical phonon is usually determined by phonon-phonon interaction. Therefore, the anomaly of the damping rate around 3 GPa can be attributed to the pressure-induced ETT, which affects the phonon dynamics.

As shown in Figs. 4(a) and 4(b), the period and corresponding frequency of the fast oscillatory component dramatically changes as Bi_2Se_3 transforms into a $C2/m$ structure at 11.5 GPa. The central frequencies of the phonon modes are determined from Lorentzian fits to the peaks in frequency domain. As a representative example in Fig. 4(b), the two extracted frequencies of 1.34 THz (~45 cm^{-1}) and 1.75 THz (~58 cm^{-1}) at 11.5 GPa are in good agreement with the A^1_g and A^2_g modes that are observed in the Raman-scattering experiments. To the best of our knowledge, this is the first time that these low-frequency phonon modes have been observed by a combination of Raman and optical pump-probe spectroscopy. Figure 4(d) summarizes the phonon frequencies extracted from $\Delta R(t)/R_0$ signals and the experimental Raman modes under different pressures from 11.5 to 18.9 GPa. Both frequencies manifest blueshift with elevating pressure due to the pressure-induced enhancement of interlayer interactions. It is noted that these two phonon modes are significantly decreased around 16 GPa and weakened gradually in $\Delta R(t)/R_0$ upon further compression, while they tend to disappear more slowly in the Raman spectra.

Finally, we comment on the pressure dependence of the acoustic phonon mode. Figure 5 shows the low-frequency components obtained by subtracting the high-frequency contributions from the residual oscillations. The low-frequency oscillations are attributed to coherent acoustic phonons arising from the pump-induced periodic modulation of the dielectric function along the c axis. According to the pulse propagation model, the frequency of acoustic phonons f_a is determined by the sound speed v, that is, $f_a = 2nv\cos(\theta)/\lambda$ [50], where n is the refraction index of Bi_2Se_3 at the pump wavelength λ, and θ is the incident angle of the pump beam. As shown in Fig. 5, the period significantly decreases with delay time due to energy relaxation of acoustic phonons [12]. For simplicity's sake, we define the time interval Δt between the second wave valley and peak as the half period of oscillation to trace the pressure evolution of the coherent acoustic phonon.

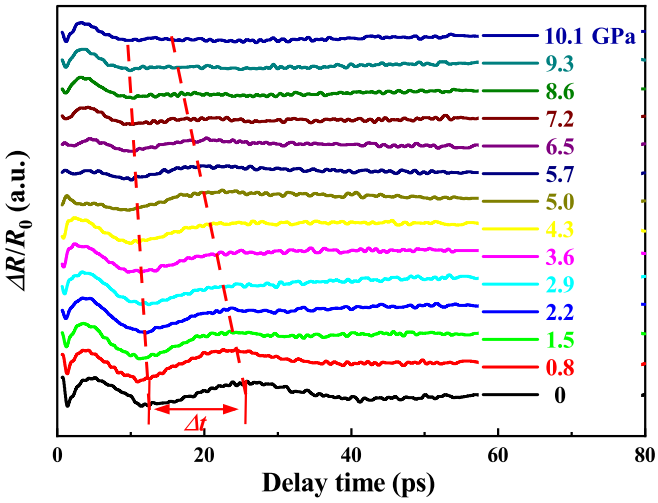

FIG. 5. Residual low-frequency oscillations at different pressures. The dashed lines in the figure are guides for the eye.

Apparently, the Δt moderately declines with increasing pressure. This phenomenon is mainly due to an increase in sound speed under pressure, as a result of the gradually decreasing interlayer distance and the increasing interlayer interaction with pressure.

IV. SUMMARY

In conclusion, we have traced the pressure evolution of carrier and phonon dynamics in Bi_2Se_3 by a combination of Raman scattering and optical pump-probe spectroscopy. Both the Raman spectra and transient reflectivity manifest discontinuous changes around 3, 11.5, 18.9, and 28 GPa, which can be attributed to the phase transitions. Detailed analysis reveals that the photocarrier relaxation time and the damping rate of the A_{1g}^1 phonon mode exhibit anomalies around 3 GPa supporting the occurrence of ETT. At higher pressure, significant evolution of quasiparticle dynamics can be attributed to the structure transitions. In addition, three low-frequency Raman-active modes, i.e., B_g^1, A_g^1, and A_g^2, are observed in the $C2/m$ phase by the Raman spectra, while the two A_g modes can also be resolved in the transient reflectivity which reveals pressure-induced blueshift in frequency. These results not only provide crucial insights into carrier-phonon interaction in Bi_2Se_3 under high pressure, but also pave the way for investigating the pressure-induced phase transitions from the transient reflection spectroscopy.

ACKNOWLEDGMENT

This work is supported by the National Natural Science Foundation of China (Grant No. 11974414) and the Synergetic Extreme Condition User Facility (SECUF).

[1] S. Kovalev, K.-J. Tielrooij, J.-C. Deinert, I. Ilyakov, N. Awari, M. Chen, A. Ponomaryov, M. Bawatna, T. V. A. G. de Oliveira, L. M. Eng, K. A. Kuznetsov, D. A. Safronenkov, G. Kh. Kitaeva, P. I. Kuznetsov, H. A. Hafez, D. Turchinovich, and M. Gensch, Terahertz signatures of ultrafast Dirac fermion relaxation at the surface of topological insulators, npj Quantum Mater. **6**, 84 (2021).

[2] D. Pesin and A. H. Macdonald, Spintronics and pseudospintronics in graphene and topological insulators, Nat. Mater. **11**, 409 (2013).

[3] H. Zhang, C.-X. Liu, X.-L. Qi, X. Dai, Z. Fang, and S.-C. Zhang, Topological insulators in Bi_2Se_3, Bi_2Te_3 and Sb_2Te_3 with a single Dirac cone on the surface, Nat. Phys. **5**, 438 (2009).

[4] Y. L. Chen, J. G. Analytis, J.-H. Chu, Z. K. Liu, S.-K. Mo, X. L. Qi, H. J. Zhang, D. H. Lu, X. Dai, Z. Fang, S. C. Zhang, I. R. Fisher, Z. Hussain, and Z.-X. Shen, Experimental realization of a three-dimensional topological insulator, Bi_2Te_3, Science **325**, 178 (2009).

[5] Y. H. Wang, H. Steinberg, P. Jarillo-Herrero, and N. Gedik, Observation of Floquet-Bloch states on the surface of a topological insulator, Science **342**, 453 (2013).

[6] H. Li, L. Sheng, D. N. Sheng, and D. Y. Xing, Chern number of thin films of the topological insulator Bi_2Se_3, Phys. Rev. B **82**, 165104 (2010).

[7] C. E. ViolBarbosa, C. Shekhar, B. Yan, S. Ouardi, E. Ikenaga, G. H. Fecher, and C. Felser, Direct observation of band bending in the topological insulator Bi_2Se_3, Phys. Rev. B **88**, 195128 (2013).

[8] Y. Xia, D. Qian, D. Hsieh, L. Wray, A. Pal, H. Lin, A. Bansil, D. Grauer, Y. S. Hor, R. J. Cava, and M. Z. Hasan, Observation of a large-gap topological-insulator class with a single Dirac cone on the surface, Nat. Phys. **5**, 398 (2009).

[9] G. Jnawali, S. Linser, I. A. Shojaei, S. Pournia, H. E. Jackson, L. M. Smith, R. F. Need, and S. D. Wilson, Revealing optical transitions and carrier recombination dynamics within the bulk band structure of Bi_2Se_3, Nano Lett. **18**, 5875 (2018).

[10] C.-W. Luo, H. J. Wang, S. A. Ku, H.-J. Chen, T. T. Yeh, J.-Y. Lin, K. H. Wu, J. Y. Juang, B. L. Young, T. Kobayashi, C.-M. Cheng, C.-H. Chen, K.-D. Tsuei, R. Sankar, F. C. Chou, K. A. Kokh, O. E. Tereshchenko, E. V. Chulkov, Yu. M. Andreev, and G. D. Gu, Snapshots of Dirac fermions near the Dirac point in topological insulators, Nano Lett. **13**, 5797 (2013).

[11] L. Braun, G. Mussler, A. Hruban, M. Konczykowski, T. Schumann, M. Wolf, M. Münzenberg, L. Perfetti, and T. Kampfrath, Ultrafast photocurrents at the surface of the three-dimensional topological insulator Bi_2Se_3, Nat. Commun. **7**, 13259 (2016).

[12] N. Kumar, B. A. Ruzicka, N. P. Butch, P. Syers, K. Kirshenbaum, J. Paglione, and H. Zhao, Spatially resolved femtosecond pump-probe study of topological insulator Bi_2Se_3, Phys. Rev. B **83**, 235306 (2011).

[13] J. Qi, X. Chen, W. Yu, P. Cadden-Zimansky, D. Smirnov, N. H. Tolk, I. Miotkowski, H. Cao, Y. P. Chen, Y. Wu, S. Qiao, and Z. Jiang, Ultrafast carrier and phonon dynamics in Bi_2Se_3 crystals, Appl. Phys. Lett. **97**, 182102 (2010).

[14] P. Sharma, D. Sharma, N. Vashistha, P. Rani, M. Kumar, S. S. Islam, and V. P. S. Awana, Ultrafast spectroscopy of

Bi_2Se_3 topological insulator, AIP Conf. Proc. **2220**, 110033 (2020).

[15] Y.-P. Lai, H.-J. Chen, K.-H. Wu, and J.-M. Liu, Temperature-dependent carrier-phonon coupling in topological insulator Bi_2Se_3, Appl. Phys. Lett. **105**, 232110 (2014).

[16] Y. D. Glinka, S. Babakiray, T. A. Johnson, A. D. Bristow, M. B. Holcomb, and D. Lederman, Ultrafast carrier dynamics in thin-films of the topological insulator Bi_2Se_3, Appl. Phys. Lett. **103**, 151903 (2013).

[17] Y. D. Glinka, S. Babakiray, T. A. Johnson, M. B. Holcomb, and D. Lederman, Effect of carrier recombination on ultrafast carrier dynamics in thin films of the topological insulator Bi_2Se_3, Appl. Phys. Lett. **105**, 171905 (2014).

[18] M. C. Wang, S. Qiao, Z. Jiang, S. N. Luo, and J. Qi, Unraveling photoinduced spin dynamics in topological insulator Bi_2Se_3, Phys. Rev. Lett. **116**, 036601 (2016).

[19] D. Hsieh, F. Mahmood, J. W. McIver, D. R. Gardner, Y. S. Lee, and N. Gedik, Selective probing of photoinduced charge and spin dynamics in the bulk and surface of a topological insulator, Phys. Rev. Lett. **107**, 077401 (2011).

[20] S. K. Saini, N. K. Tailor, P. Sharma, L. Tyagi, N. Vashistha, R. Yadav, A. K. Chaudhary, S. Satapathi, and M. Kumar, Revealing the substrate dependent ultrafast phonon dynamics in Bi_2Se_3 thin films, Adv. Mater. Interfaces **10**, 2201650 (2023).

[21] Y. Kim, X. Chen, Z. Wang, J. Shi, I. Miotkowski, Y. P. Chen, P. A. Sharma, A. L. Lima Sharma, M. A. Hekmaty, Z. Jiang, and D. Smirnov, Temperature dependence of Raman-active optical phonons in Bi_2Se_3 and Sb_2Te_3, Appl. Phys. Lett. **100**, 071907 (2012).

[22] Q. Liu, R. Shao, N. Li, W. Liang, X. Yang, S. N. Luo, and Y. Zhao, Anharmonicity of Bi_2Se_3 revealed by fs transient optical spectroscopy, Appl. Phys. Lett. **115**, 201902 (2019).

[23] Y. D. Glinka, S. Babakiray, T. A. Johnson, M. B. Holcomb, and D. Lederman, Acoustic phonon dynamics in thin-films of the topological insulator Bi_2Se_3, J. Appl. Phys. **117**, 165703 (2015).

[24] G. Prakash, K. Pal, M. Jain, U. V. Waghmare, and A. K. Sood, Origin of the thermal expansion anomaly in layered Bi_2X_3 topological insulators: Ultrafast time-resolved pump-probe experiments and theory, Phys. Rev. B **96**, 075109 (2017).

[25] Y. L. Wu, X. Yin, J. Z. L. Hasaien, Z. Y. Tian, Y. Ding, and J. Zhao, On-site *in situ* high-pressure ultrafast pump-probe spectroscopy instrument, Rev. Sci. Instrum. **92**, 113002 (2021).

[26] B. H. Yu, Z. Y. Tian, F. Sun, D. C. Peets, X. D. Bai, D. L. Feng, and J. Zhao, Ultrafast quasiparticle dynamics and coherent phonon in nodal line topological material LaBi, Opt. Express **28**, 15855 (2020).

[27] K. Zhang, F. Su, D. Liu, W. Wang, Y. Zhang, Z. Zeng, Z. Qu, and A. F. Goncharov, Probing the electronic topological transitions of WTe_2 under pressure using ultrafast spectroscopy, arXiv:2303.04974.

[28] X. Hong, M. Newville, Y. Ding, T. Irifune, G. Gu, and H.-K. Mao, Distinct intermediate states in the isostructural *R*-3*m* phase of the topological insulator Bi_2Se_3 at high pressure, Phys. Rev. B **101**, 214107 (2020).

[29] R. Vilaplana, D. Santamaría-Pérez, O. Gomis, F. J. Manjón, J. González, A. Segura, A. Muñoz, P. Rodríguez-Hernández, E. Pérez-González, V. Marín-Borrás, V. Muñoz-Sanjose, C. Drasar, and V. Kucek, Structural and vibrational study of Bi_2Se_3 under high pressure, Phys. Rev. B **84**, 184110 (2011).

[30] F. J. Manjón, R. Vilaplana, O. Gomis, E. Pérez-González, D. Santamaría-Pérez, V. Marín-Borrás, A. Segura, J. González, P. Rodríguez-Hernández, A. Muñoz, C. Drasar, V. Kucek, and V. Muñoz-Sanjosé, High-pressure studies of topological insulators Bi_2Se_3, Bi_2Te_3, and Sb_2Te_3, Phys. Status Solidi B **250**, 669 (2013).

[31] Z. Yu, L. Wang, Q. Hu, J. Zhao, S. Yan, K. Yang, S. Sinogeikin, G. Gu, and H.-K. Mao, Structural phase transitions in Bi_2Se_3 under high pressure, Sci. Rep. **5**, 15939 (2015).

[32] X. Hao, H. Zhu, Z. Guo, H. Li, Y. Gong, and D. Chen, Local insight to the structural phase transition sequence of Bi_2Se_3 under quasi-hydrostatic and nonhydrostatic pressure, J. Phys.: Condens. Matter **33**, 215402 (2021).

[33] H. Zhu, J. Dong, P. Li, Y. Wang, Z. Guo, X. Shan, Y. Gong, P. An, X. Li, J. Zhang, and D. Chen, Bi-centric view of the isostructural phase transitions in α-Bi_2Se_3 and α-Bi_2Te_3, Phys. Status Solidi B **254**, 1700007 (2017).

[34] J. J. Hamlin, J. R. Jeffries, N. P. Butch, P. Syers, D. A. Zocco, S. T. Weir, Y. K. Vohra, J. Paglione, and M. B. Maple, High pressure transport properties of the topological insulator Bi_2Se_3, J. Phys.: Condens. Matter **24**, 035602 (2012).

[35] J. Zhang, Y. Han, C. Liu, X. Zhang, F. Ke, G. Peng, Y. Ma, Y. Ma, and C. Gao, Semiconductor-to-metal transition of Bi_2Se_3 under high pressure, Appl. Phys. Lett. **105**, 062102 (2014).

[36] H. Cheng, J. Zhang, Y. Li, G. Li, and X. Li, Structure determination of the high-pressure phases of topological insulator Bi_2Se_3 using experiments and calculations, J. Appl. Phys. **121**, 225902 (2017).

[37] J. Zhang, Z. Peng, A. Soni, Y. Zhao, Y. Xiong, B. Peng, J. Wang, M. S. Dresselhaus, and Q. Xiong, Raman spectroscopy of few-quintuple layer topological insulator Bi_2Se_3 nanoplatelets, Nano Lett. **11**, 2407 (2011).

[38] A. Dewaele, A. B. Belonoshko, G. Garbarino, F. Occelli, P. Bouvier, M. Hanfland, and M. Mezouar, High-pressure–high-temperature equation of state of KCl and KBr, Phys. Rev. B **85**, 214105 (2012).

[39] S. Rast, M. L. Schneider, M. Onellion, X. H. Zeng, W. Si, X. X. Xi, M. Abrecht, D. Ariosa, D. Pavuna, Y. H. Ren, G. Lüpke, and I. Perakis, Evidence for two coupled subsystems in the superconducting state of $La_{2-x}Sr_xCuO_4$, Phys. Rev. B **64**, 214505 (2001).

[40] J. A. Sobota, S. Yang, J. G. Analytis, Y. L. Chen, I. R. Fisher, P. S. Kirchmann, and Z.-X. Shen, Ultrafast optical excitation of a persistent surface-state population in the topological insulator Bi_2Se_3, Phys. Rev. Lett. **108**, 117403 (2012).

[41] K. Kirshenbaum, P. S. Syers, A. P. Hope, N. P. Butch, J. R. Jeffries, S. T. Weir, J. J. Hamlin, M. B. Maple, Y. K. Vohra, and J. Paglione, Pressure-induced unconventional superconducting phase in the topological insulator Bi_2Se_3, Phys. Rev. Lett. **111**, 087001 (2013).

[42] W.-K. Tse and S. Das Sarma, Energy relaxation of hot Dirac fermions in graphene, Phys. Rev. B **79**, 235406 (2009).

[43] K. Zhang, J. Xie, J. Yang, H. Jiang, S. Zhang, Z. Zeng, X. Chen, T. Wang, and F. Su, Nonequilibrium electron and lattice dynamics of Sb_2Te_3 under pressure, Phys. Rev. B **105**, 195109 (2022).

[44] S. K. Saha, H. Banerjee, and M. Kumar, Topological transitions to Weyl states in bulk Bi_2Se_3: Effect of hydrostatic pressure and doping, J. Appl. Phys. **129**, 085103 (2021).

[45] H. Yamaoka, H. O. Jeschke, X. Yang, T. He, H. Goto, N. Hiraoka, H. Ishii, J. Mizuki, and Y. Kubozono, Electronic structures of Bi_2Se_3 and $Ag_xBi_2Se_3$ under pressure studied by high-resolution x-ray absorption spectroscopy and density functional theory calculations, Phys. Rev. B **102**, 155118 (2020).

[46] N. Li, W. Liang, and S.-N. Luo, Hot carrier dynamics and phonon anharmonicity of $ZrTe_5$ revealed with femtosecond transient optical spectroscopy, Phys. Rev. B **101**, 014304 (2020).

[47] X. Xie, J. Ding, B. Wu, H. Zheng, S. Li, J. He, Z. Liu, J.-T. Wang, and Y. Liu, Unveiling layer-dependent interlayer coupling and vibrational properties in $MoTe_2$ under high pressure, Phys. Rev. B **108**, 155302 (2023).

[48] O. Gomis, R. Vilaplana, F. J. Manjón, P. Rodríguez-Hernández, E. Pérez-González, A. Muñoz, V. Kucek, and C. Drasar, Lattice dynamics of Sb_2Te_3 at high pressures, Phys. Rev. B **84**, 174305 (2011).

[49] R. Vilaplana, O. Gomis, F. J. Manjón, A. Segura, E. Pérez-González, P. Rodríguez-Hernández, A. Muñoz, J. González, V. Marín-Borrás, V. Muñoz-Sanjosé, C. Drasar, and V. Kucek, High-pressure vibrational and optical study of Bi_2Te_3, Phys. Rev. B **84**, 104112 (2011).

[50] C. Thomsen, H. T. Grahn, H. J. Maris, and J. Tauc, Surface generation and detection of phonons by picosecond light pulses, Phys. Rev. B **34**, 4129 (1986).